# QUEEG: A Monte Carlo Event Generator for Quasielastic Scattering on Deuterium

G.P. Gilfoyle[1], J.D. Lachniet[2], and O. Alam[1]

[1] *University of Richmond, Richmond, VA*
[2] *Areté Associates, Arlington, VA*

September 5, 2014

**Abstract**

We have developed a simulation of quasielastic electron scattering off nucleons in deuterium. The original code was developed by J.Lachniet for the analysis of the CLAS6 $G_M^n$ experiment. The Fermi motion of the nucleons creates an effective beam energy different from the laboratory one as seen from the rest frame of the moving nucleon. This effective beam energy is used with the Hulthen distribution (for the magnitude of the Fermi motion) and the elastic form factors (for the elastic scattering in the nucleon rest frame) to calculate a relative probability as a function of the Fermi momentum $p_f$ and $\theta_N$, the direction of the moving nucleon relative to the beam. The Fermi 3-momentum $\vec{p}_f$ is selected randomly from this distribution, the electron scattering angle is chosen from the nucleon rest frame and boosted back to the lab. An option was added to QUEEG to include an asymmetric distribution in the azimuthal angle between the scattering plane (defined the incoming and scattered electrons) and the reaction plane (defined by the final nucleon momenta). Another option simulates a realistic event vertex distribution for a cylindrical target. Examples of the use of the event generator are shown. The source and Makefiles are available in the CLAS12 repository.

# 1 Introduction

We have developed an event generator for quasielastic scattering off nucleons in deuterium. This work was motivated by the need to realistically simulate quasielastic scattering off deuterium for the CLAS6 measurement of the neutron magnetic form factor, $G_M^n$ [1, 2, 3] and for the approved CLAS12 experiment E12-07-104 entitled 'Measurement of the Neutron Magnetic Form Factor at High $Q^2$ Using the Ratio Method on Deuterium' [4]. In both experiments the ratio of $e-n$ to $e-p$ in quasielastic scattering is used to extract $G_M^n$, the neutron magnetic form factor. This ratio method was successfully applied in the CLAS6 experiment for beam energies of 4.2 GeV and 2.6 GeV [1, 2, 3]. It is also been used to simulate the helicity asymmetry in the CLAS-Approved Analysis entitled 'Out-of-Plane Measurements of the Structure Functions of the Deuteron'. Here, the helicity asymmetry $A_h$ can be extracted from $e-p$ scattering to isolate the little-known fifth structure of the deuteron. The first version of the code was written by J.Lachniet and dubbed QUEEG for 'QUasi-Elastic Event Generator' [2]. In this CLAS NOTE we discuss the necessary background (Section 2) and how we simulate quasielastic $e-p$ and $e-n$ events on deuterium (Section 3). We then present results from simulations of the CLAS6 and CLAS12 detectors (Section 4) and finish with a section on building the code and running it (Section 5).

# 2 Elastic, Electromagnetic Nucleon Form Factors

The nucleon elastic form factors are defined through the matrix elements of the electromagnetic current $J_\mu = \overline{\psi}\gamma_\mu\psi$ as

$$\langle N(P')|J_\mu(0)|N(P)\rangle = \overline{u}(P')\left(\gamma_\mu F_1(Q^2) + \frac{i\sigma_{\mu\nu}q^\nu\kappa}{2M}F_2(Q^2)\right)u(P) \tag{1}$$

where $P$ and $P'$ are the initial and final nucleon momenta, $q = P - P'$, $Q^2 = -q^2$, $M$ is the nucleon mass, $\kappa$ is the anomalous magnetic moment, and $F_1$ and $F_2$ are scalar functions of $Q^2$ that characterize the internal structure of the nucleon. These are the Dirac and Pauli form factors, respectively. The differential cross section for elastic electron-nucleon scattering can then be calculated in the laboratory frame as [5]

$$\frac{d\sigma}{d\Omega} = \sigma_{Mott}\left[\left(F_1^2 + \frac{\kappa^2Q^2}{4M^2}F_2^2\right) + \frac{Q^2}{2M^2}\left(F_1 + \kappa F_2\right)^2\tan^2\left(\frac{\theta_e}{2}\right)\right] \tag{2}$$

where $\theta_e$ is the electron scattering angle, and $\sigma_{Mott}$ is

$$\sigma_{Mott} = \frac{\alpha^2E'\cos^2(\frac{\theta}{2})}{4E^3\sin^4(\frac{\theta}{2})} \tag{3}$$

where $E$ is the beam energy and $E'$ is the scattered electron energy. It is convenient to define different electromagnetic form factors that are related to the charge and magnetization density of the nucleon in the appropriate kinematics. These so-called Sachs form factors are defined as

$$G_E = F_1 - \frac{\kappa Q^2}{4M^2}F_2 \qquad G_M = F_1 + \kappa F_2 \tag{4}$$

so Equation 2 can be written as

$$\frac{d\sigma}{d\Omega} = \sigma_{Mott}\left(G_E^2 + \frac{\tau}{\epsilon}G_M^2\right)\left(\frac{1}{1+\tau}\right) \tag{5}$$

where

$$\tau = \frac{Q^2}{4M^2} \qquad \text{and} \qquad \epsilon = \frac{1}{1+2(1+\tau)\tan^2(\frac{\theta}{2})} \quad . \tag{6}$$

# 3 Simulating Quasielastic Scattering on Deuterium

To simulate the quasielastic production we treat the deuteron as composed of two, on-shell nucleons, one of which will act as a spectator in the interaction. The quasielastic interaction is then elastic scattering with the target nucleon, but we must also add the effect of the Fermi motion of this target nucleon within the deuteron. This approach enables us to take advantage of existing data on electron scattering on the proton and the deuteron.

We start with the nucleon elastic electromagnetic form factors. We use Equations 2-6 and make the following assumptions about the form factors

$$G_E^p \approx G_D = \frac{1}{(1+Q^2/\Delta)^2} \qquad G_M^p \approx \mu_p G_D \qquad G_M^n \approx \mu_n G_D \qquad G_E^n = \frac{\mu_n \tau G_D}{1+\eta\tau} \tag{7}$$

where $\mu_n$ and $\mu_p$ are the neutron and proton magnetic moments, $\Delta = 0.71$ $(\mathrm{GeV/c})^2$, and $\eta = 5.6$ (from the Galster parameterization [6]). The number of quasielastic events in a particular $Q^2$ bin is calculated from these elastic form factors. Next, the Fermi momentum $\vec{p}_f$ for one of the nucleons is chosen at random (the spectator nucleon has momentum $-\vec{p}_f$) and we simulate the kinetics of the scattering. The magnitude of the nucleon momentum $|\vec{p}_f|$ inside the deuteron is chosen from the Hulthen distribution shown in Figure 1 and the direction is isotropic [7].

We also have to account for combined effect of the Fermi motion and the beam energy dependence of the elastic cross section. A nucleon whose Fermi motion is directed towards the incoming electron will observe effectively a higher energy beam in its rest frame and (because of the elastic cross section dependence on the beam energy) will have a lower cross section for interacting. Conversely, a nucleon 'running away' from the beam will see a lower apparent beam energy and have a higher cross section.

For a given choice of Fermi momentum $p_f$ and nucleon polar angle $\cos\theta_N$ there is an effective beam energy in the rest frame of the moving nucleon. The angle $\theta_N$ here is the angle between the direction of the moving target nucleon and the beam axis in the laboratory. The size of the cross section at this effective beam energy in the nucleon rest frame and the Hulthen distribution will determine the relative weight of this $p_f - \cos\theta_N$ combination. At each effective beam energy in the quasielastic case the Brash parameterization [8] of the nucleon cross section is used to obtain the cross section dependence on the electron scattering angle. This angular dependence is integrated over the CLAS12 angular acceptance to obtain the weighting due to the effective-beam-energy effect at each $p_f - \cos\theta_N$ point. Multiplying this effective-beam-energy weight with the Hulthen distribution at each $p_f - \cos\theta_N$ point yields the weight functions for electron-proton and electron-neutron scattering. The results

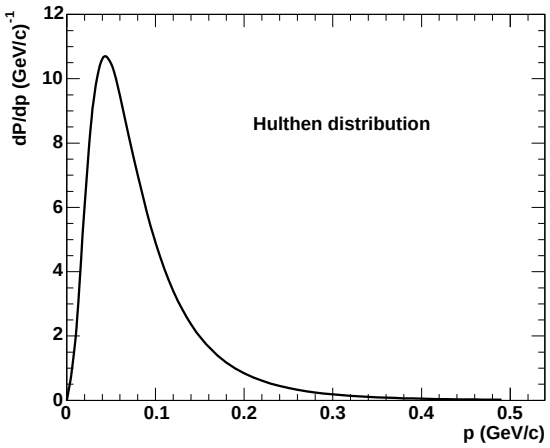


Figure 1: Hulthen distribution representing the nucleon Fermi momentum inside the deuteron.

are shown in Figure 2. The Hulthen distribution produces a long ridge in the range of the Fermi momentum $p_f \approx 0.04 - 0.05\ GeV/c$ and the cross section dependence on the effective beam energy creates a downward slope along this ridge from forward to backward angles. We can now use these functions to choose the Fermi momentum $\vec{p}_f$ for the quasielastic case.

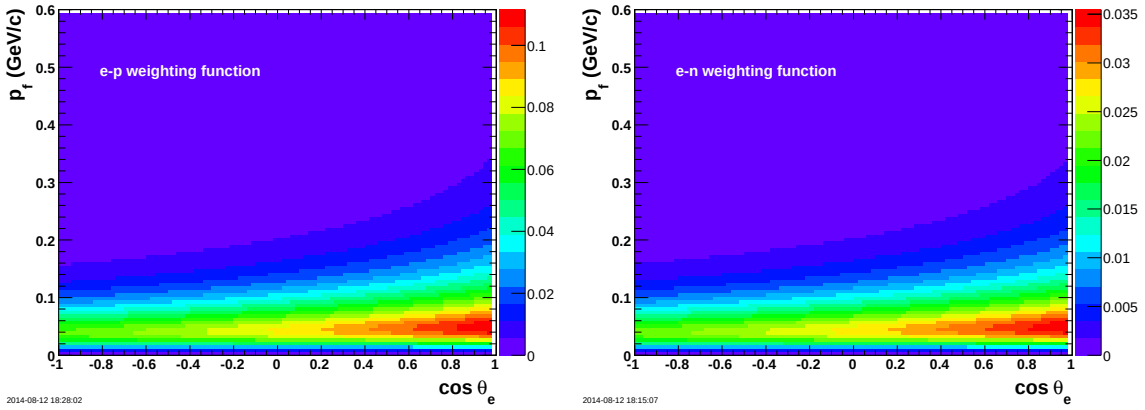


Figure 2: Plot of the weighting function for electron-proton (left-hand panel) and electron-neutron (right-hand panel) scattering. The beam energy is 11 GeV. The angle $\theta_N$ is the angle between the direction of the moving target nucleon and the beam axis in the laboratory.

The algorithm for simulating the Fermi motion is as follows.

1. An $e - p$ or $e - n$ event is chosen randomly in a proportion selected by the user.

2. The magnitude of the Fermi momentum $p_f$ and $\cos\theta_N$ are picked from the distributions in Figure 2. The azimuthal angle $\phi_f$ of the nucleon is usually chosen from a uniform,

random distribution in the range $\phi_f = 0 - 2\pi$. Variations on this method will be discussed below.

3. The electron scattering angle is chosen randomly according to the dependence of the cross section on scattering angle $\theta_e$ in the rest frame of the moving nucleon target as shown in Figure 3. The azimuthal angle $\phi_e$ is chosen randomly from a uniform distribution in the range $\phi_e = 0 - 2\pi$ rad.

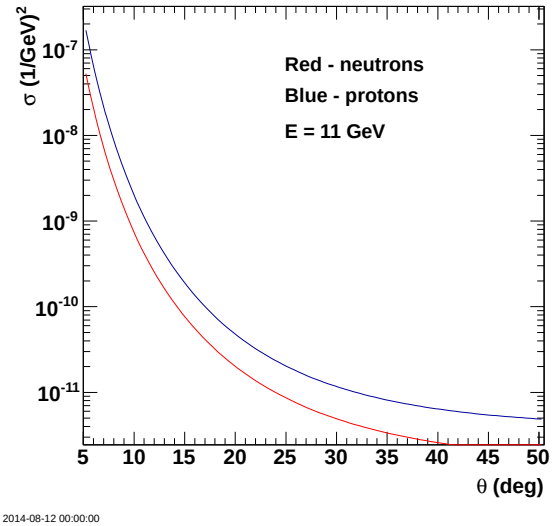


Figure 3: Plot of the cross section for $e - p$ (blue) and $e - n$ (red) scattering as a function of angle $\theta$.

4. The rest frame scattering angles are boosted back to the lab frame.

5. To ensure that the conservation laws are satisfied, the value of the scattered electron momentum is adjusted. We start with the value of the scattered electron energy in the nucleon rest frame $E'$ and apply 3-momentum conservation so

$$E\hat{z} + \vec{p}_f = E'\hat{e} + \vec{p}_N \tag{8}$$

where $E$ is the beam energy, $\hat{z}$ is along the beam axis, $\hat{e}$ is the direction of the scattered electron in the lab frame, and $\vec{p}_N$ is the scattered nucleon momentum in the lab. The spectator nucleon 3-momentum is $-\vec{p}_f$ for the initial and final states. One obtains the value of $\vec{p}_N$ by solving Eq. 8 and then calculates a new value of $E'$ by applying energy conservation.

$$E + M_D = E_S + E_N + E' \tag{9}$$

where $M_D$ is the deuteron mass, $E_S$ is the spectator energy and $E_N$ is the scattered nucleon energy. This procedure is followed iteratively until the value for $E'$ converges.

We now discuss how the code was modified to simulate the helicity asymmetry for deuterium. The reaction $^2\mathrm{H}(\vec{e}, e'p)n$ reaction was used. The cross section for a polarized electron beam and unpolarized target can be written as

$$\frac{d^3\sigma}{dE'd\Omega d\Omega_p} = \sigma_{Mott} K \left(\rho_{00} f_{oo} + \rho_{11} f_{11} + \rho_{01} f_{01} \cos\phi_{pq} + \rho_{1-1} f_{1-1} \cos 2\phi_{pq} + h\rho'_{01} f'_{01} \sin\phi_{pq}\right) \tag{10}$$

where $\Omega$ is the electron solid angle, $\Omega_p$ is the proton solid angle, the $\rho_{ij}$ are the components of the lepton tensor, $f_{ij}$ are the structure functions, $K = (W^2 - M^2)/2M$, $W$ is the invariant mass, $M$ is the nucleon mass, and $\phi_{pq}$ is the angle between the scattering plane (the incoming and scattered electron 3-momenta define the scattering plane) and the reaction plane (the 3-momentum transfer $\vec{q} = \vec{p}_{e'} - \vec{p}_e$ and the final proton 3-momentum $\vec{p}_p$ define the reaction plane). See Figure 4. The last term of the right-hand-side of Eq. 10 has a factor $h = \pm 1$ depending on the helicity of the beam.

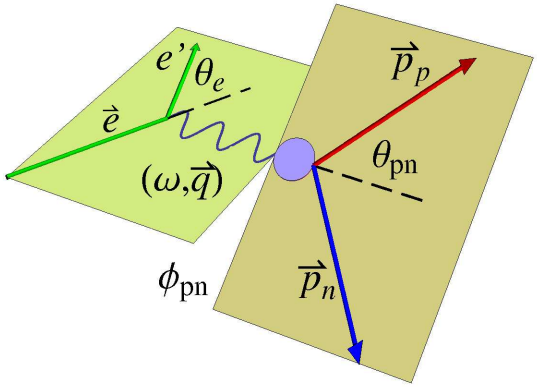


Figure 4: Kinematic quantities for $^2\mathrm{H}(\vec{e}, e'p)n$ are shown. The momentum of the particle is $\vec{p}$ and the residual is $\vec{q}$. The energy transfer is $\omega = E - E'$.

The helicity asymmetry can be constructed from

$$A_h = \frac{\sigma^+ - \sigma^-}{\sigma^+ + \sigma^-} \propto f'_{01} \sin\phi_{pq} \tag{11}$$

where the $\sigma^\pm$ correspond to the differential cross in Eq. 10 for different values of the helicity $h$. The proportionality can be shown by noting the helicity-independent part of the cross section will cancel in the numerator while the helicity-dependent piece cancels in the denominator. This makes Eq. 11 a probe of the so-called fifth structure function $f'_{01}$ which is the imaginary part of the longitudinal-transverse ($LT$) interference.

Simulating the impact of the fifth structure function requires altering the selection of the azimuthal angle from a uniform distribution that was described above. The procedure is the following.

1. The magnitude of the the proton Fermi momentum $|\vec{p}_f|$ is chosen randomly weighted by the distributions in Figure 2 as described above.

2. The Fermi momentum is used to select the amplitude of the sinusoidal oscillation. We fit our measured results for a closely related asymmetry $A'_{LT}$ as a function of $p_f$ and use these results to pick the amplitude of the sinusoidally-varying, helicity-dependent part of the cross section. See the left-hand panel of Figure 5. It shows the fitted curve from the data (black curve) and the asymmetry of the thrown events (red points) before they are processed by the CLAS6 simulation package *gsim*. The blue points are the result of averaging the fitted curve (black) over the $p_f$ bin. There is excellent agreement between the input to the event generator (blue points) and the output (red points).

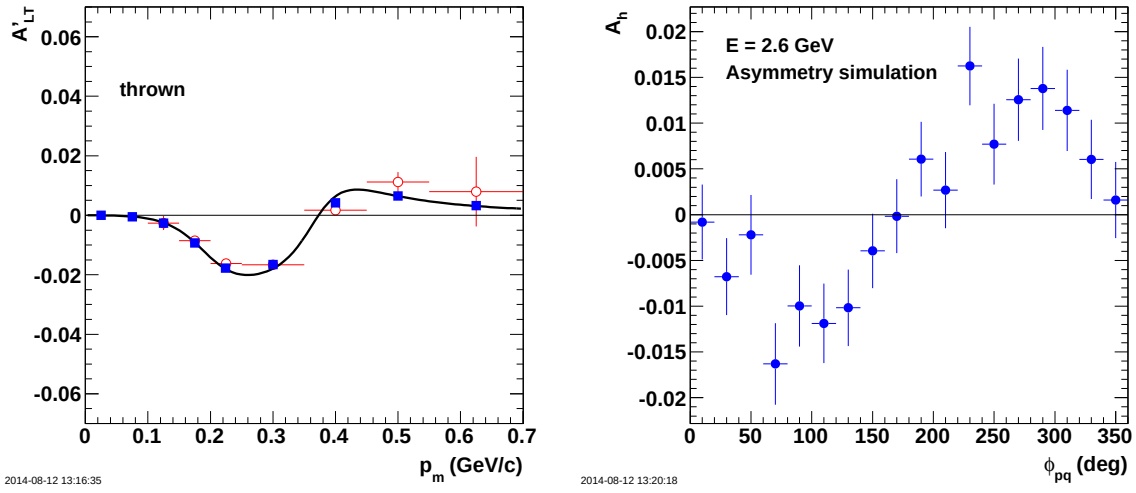


Figure 5: Simulation of the helicity asymmetry in $^2\mathrm{H}(\vec{e}, e'p)n$ reaction with QUEEG. The left-hand panel shows the amplitude of the asymmetry used as input (black curve), the same asymmetry averaged over the momentum bin (blue points), and the output of QUEEG (red points). The event generator output agrees with the input asymmetry. The left-hand panel shows the asymmetry for $p_f = 0.22$ GeV as a function of $\phi_{pn}$.

3. The probability distribution function for $\phi_{pq}$ is treated as a sum of a uniform part and the sinusoidally-oscillating part and we apply von Neumann rejection to randomly select values of $\phi_{pq}$ with the desired distribution. Some results are shown in the right-hand panel of Figure 5. It shows the asymmetry from the thrown events produced by QUEEG. The asymmetry has the expected sinusoidal shape.

# 4 Results

We now show some results from QUEEG to demonstrate its use. In the analysis of the CLAS6 $G_M^n$ measurement the event generator was used to calculate the effect of the Fermi motion

on the determination of $G_M^n$ [1, 2, 3]. Simulated events that would be detected by CLAS6 without the presence of Fermi motion were compared with ones with the Fermi motion turned on. In some of those latter events, the nucleon trajectory through the detector would be altered so that it would fall out of the active area of CLAS6 and be lost. This effect was corrected using the results of QUEEG and the impact is shown in Figure 6. The correction for these Fermi losses makes the extraction of $G_M^n$ consistent across different detectors and different run conditions.

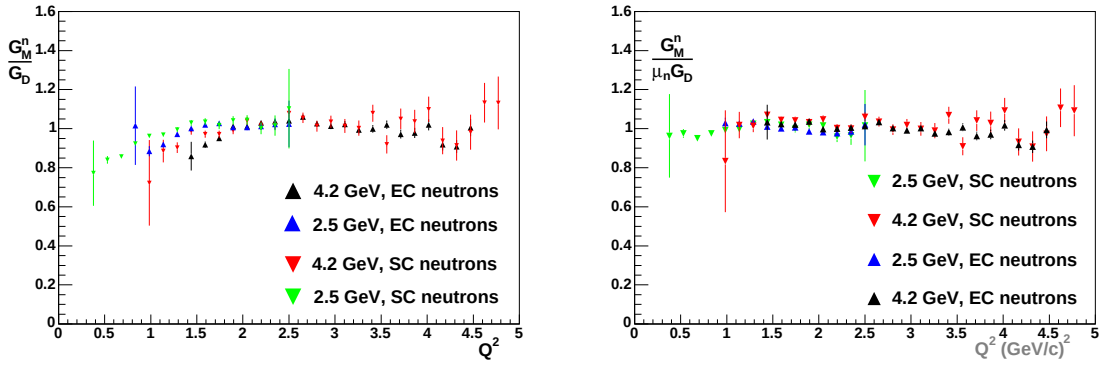


Figure 6: Comparison of CLAS6 extraction of $G_M^n$ without (left-hand panel) and including (right-hand panel) the Fermi motion correction using different detector subsystems and at different beam energies. Plots are from J.D.Lachniet thesis [2].

The QUEEG event generator was used to simulate the $Q^2$ dependence and $W$-dependence for the approved, CLAS12 proposal to measure $G_M^n$ [4]. As high $Q^2$ the width of the elastic peak in the $W^2$ distribution increases and overlaps with the inelastic production. QUEEG and other event generators were used to demonstrate that we would be able to separate the quasielastic and inelastic events in CLAS12. This result in shown in Figure 7. The left-hand panel shows the separate quasielastic (red), inelastic (green), and total (black) spectra. In the right-hand panel a 'hermiticity cut' is turned on requiring no other particles be detected in CLAS12 and reducing the background from inelastic events. Using QUEEG and other codes we showed the quasielastic events could still be separated with CLAS12 at these kinematics.

We also note the use of QUEEG in validating the analysis of the CLAS-Approved Analysis shown in Figure 5. The left-hand panels shows the amplitude of the asymmetry from a fit to our data (black curve), the same amplitude averaged over the momentum bin (blue points), and the output from QUEEG (red points). The blue points represent the input used to generate the asymmetry as described in Section 3. There is excellent agreement between the input and the results of the QUEEG calculation.

# 5 Building and Running QUEEG

To build and run QUEEG requires a Linux operating system with ROOT installed [9] and GNU Make. The code here has been built and tested on Centos 6.4, Fedora 16, and RHEL

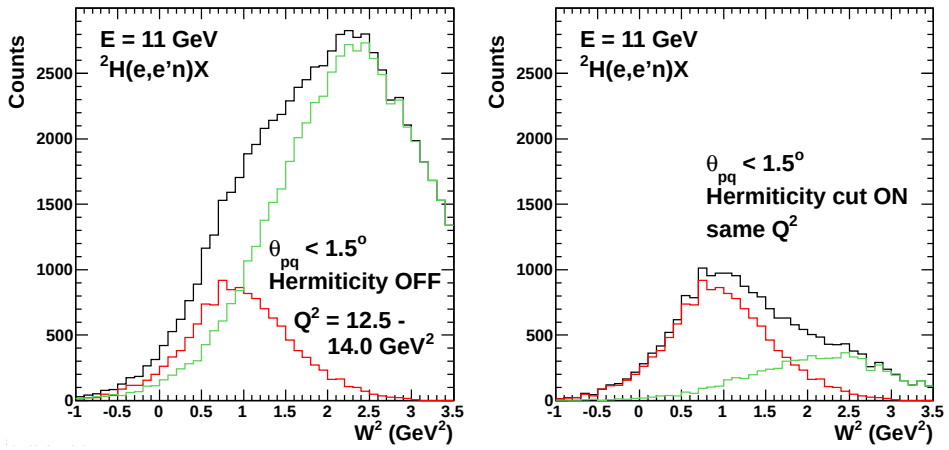


Figure 7: High $Q^2$ application of QUEEG for JLab proposal E12-07-104 [4]. The red histogram in each panel shows the broad quasielastic peak present at high $Q^2$ calculated with QUEEG. The two panels show the impact of a requirement on the simulated data that no additional partices are detected in CLAS12.

6.4. The Makefile uses `root-config` to locate the necessary ROOT libraries and include files. If that is not available or you need different libraries and/or include files, then the Make variables ROOTLIBS and ROOTINCS have to be set by hand in the Makefile. The steps to obtain and build the code are the following.

1. Check out the code from the repository in the directory */home/<you>/*.

   ```
   svn co https://clas12svn.jlab.org/repos/users/gilfoyle/qeDsim/
   ```

   This command will create a new subdirectory *qeDsim* in the directory where the command was issued.

2. Set an environment variable in tcsh

   ```
   setenv TOP_DIR /home/<you>/qeDsim/
   ```

   or bash shells.

   ```
   TOP_DIR= /home/<you>/qeDsim/ export TOP_DIR
   ```

3. Go to the source directory and issue the *make* command.

   ```
   cd qeDsim/src/queeg
   make
   ```

   If you have troubles contact gilfoyle@jlab.org.

The code is run from the command line and has the following options listed in Table 1 below. It is worth explaining some of the details of several of the options. The '-I' option sets the torus current of the magnet. This value is used to select the scattered electron angular range for the simulation. Different torus settings are associated with different angle ranges and the minimum angle, in particular, excludes many events that would not hit the active

| Option | Argument or function |
|---|---|
| -h | Print this message |
| -o | Name of output text file |
| -E | Beam energy in GeV (4.2 is default) |
| -I | Torus Current (3375A is default) as a positive number |
| -N | Number of events to generate |
| -F | Neutron fraction of events (0 to 1, default is 0.5) |
| -R | torus current is a negative number |
| -H | helicity sign is a negative number |
| -V | ALTp: 0 - no effect, 1 - normal torus polarity, 2 - reversed. |
| -L | Output in the LUND format |
| -B | Target Center in cm |
| -S | Target Length in cm |
| -r | Target Radius in cm |
| -D | Minimum electron scattering angle queeg will output |
| -U | Maximum electron scattering angle queeg will output |

Table 1: QUEEG command line options.

area of the detector. This exclusion reduces the time needed for the simulation. Options '-H' and '-V' are associated with the simulation of the fifth structure function discussed in Section 3. The '-V' option chooses among two different $p_f$-dependent, asymmetry functions that were extracted from CLAS6 measurements. Options '-B', '-S', and '-r' are used to simulate the vertex distribution of events in a real target. It is assumed the target is a cylinder with center specified by option '-B', length '-S', and radius '-r'.

There are two choices for the output format. The default format is in Table 2 where line 1 contains the number of particles in the event and line 2 contains the Geant particle ID code for an electron (3), and the energy and 3-momentum of the electron. Line 3 contains the vertex of the track. Line 4 holds the Geant particle ID code for the emitted nucleon, and its energy and 3-momentum and line 5 holds the vertex of this track (same as the electron). The other event format is the LUND format. It consists of a header line and a particle line for each track. See Table 3.

| Line | Entry |
|---|---|
| 1 | 2 |
| 2 | 3, $E'$, $p_{ex}$, $p_{ey}$, $p_{ez}$ |
| 3 | $V_x$, $V_y$, $V_z$ |
| 4 | $ID$, $E_N$, $p_{Nx}$, $p_{Ny}$, $p_{Nz}$ |
| 5 | $V_x$, $V_y$, $V_z$ |

Table 2: Default output format.

| Column | Entry |
|---|---|
| 1 | number of particles in event |
| 2 | number of target nucleons |
| 3 | number of target neutrons |
| 4 | target polarization |
| 5 | beam polarization |
| 6 | Bjorken $x$ |
| 7 | $y = \nu/E$ |
| 8 | $W^2$ |
| 9 | $Q^2$ |
| 10 | $\nu$ |

| Column | Entry |
|---|---|
| 1 | index |
| 2 | charge(e) |
| 3 | type |
| 4 | PDG ID |
| 5 | parent line |
| 6 | daughter line |
| 7 | $p_x$ |
| 8 | $p_y$ |
| 9 | $p_z$ |
| 10 | energy |
| 11 | mass |
| 12 | $V_x$ |
| 13 | $V_y$ |
| 14 | $V_z$ |
| 15 | production time |
| 16 | lifetime |

Table 3: Lund output format.

# References

[1] J. Lachniet, A. Afanasev, H. Arenhövel, W. K. Brooks, G. P. Gilfoyle, D. Higinbotham, S. Jeschonnek, B. Quinn, M. F. Vineyard, et al. Precise Measurement of the Neutron Magnetic Form Factor $G_M^n$ in the Few-GeV$^2$ Region. *Phys. Rev. Lett.*, 102(19):192001, 2009.

[2] Jeffrey Douglas Lachniet. *A High Precision Measurement of the Neutron Magnetic Form Factor Using the CLAS Detector*. PhD thesis, Carnegie-Mellon University, Pittsburgh, PA, USA, 2005.

[3] J.D. Lachniet, W.K. Brooks, G.P. Gilfoyle, B. Quinn, and M.F. Vineyard. A high precision measurement of the neutron magnetic form factor using the CLAS detector. CLAS Analysis Note 2008-103, Jefferson Lab, 2008.

[4] G.P. Gilfoyle, W.K. Brooks, S. Stepanyan, M.F. Vineyard, S.E. Kuhn, J.D. Lachniet, L.B. Weinstein, K. Hafidi, J. Arrington, D. Geesaman, R. Holt, D. Potterveld, P.E. Reimer, P. Solvignon, M. Holtrop, M. Garcon, S. Jeschonnek, and P. Kroll. Measurement of the Neutron Magnetic Form Factor at High $Q^2$ Using the Ratio Method on Deuterium. E12-07-104, Jefferson Lab, Newport News, VA, 2007.

[5] M. N. Rosenbluth. High Energy Elastic Scattering of Electrons on Protons. *Phys. Rev.*, 79(4):615–619, Aug 1950.

[6] S. Galster et al. *Nucl. Phys. B*, 32:221, 1971.

[7] F. Gross. *Relativistic Quantum Mechanics and Field Theory.* Wiley, New York, NY, 1993.

[8] E. J. Brash, A. Kozlov, S. Li, and G. M. Huber. New empirical fits to the proton electromagnetic form factors. *Phys. Rev.*, C65:051001, 2002.

[9] R. Brun and F. Rademakers. Root - an object oriented data analysis framework. In *Nucl. Inst. & Meth. in Phys. Res.*, volume A389, Lausanne, 1997.